

# AN *RXTE* SURVEY OF LONG-TERM X-RAY VARIABILITY IN SEYFERT 1 GALAXIES

A. Markowitz & R. Edelson

agm,rae@astro.ucla.edu

U.C.L.A. Department of Astronomy; Los Angeles, CA 90095-1562; USA

## ABSTRACT

Data from the first three years of *RXTE* observations have been systematically analyzed to yield a set of 300 day, 2-10 keV light curves with similarly uniform,  $\sim 5$  day sampling, for a total of nine Seyfert 1 galaxies. This is the first X-ray variability survey to consistently probe time scales longer than a few days in a large number of AGN. Comparison with *ASCA* data covering a similar band but much shorter ( $\lesssim 1$  day) time scales shows that all the AGN are more strongly variable on long time scales than on short time scales. This increase is greatest for the highest-luminosity sources. The well-known anticorrelation between source luminosity and variability amplitude is both stronger and shallower in power-law slope when measured on long time scales. This is consistent with a picture in which the X-ray variability of Seyfert 1s can be described by a single, universal fluctuation power density shape for which the cutoff moves to longer time scales for higher luminosity sources. All of the Seyfert 1s exhibit stronger variability in the relatively soft 2-4 keV band than in the harder 7-10 keV band. This effect is much too pronounced to be explained by simple models based on either the dilution of the power-law continuum by the Compton reflection component or on the hard X-rays being produced in a static, pair-dominated, plane-parallel Comptonizing corona.

*Subject headings:* galaxies: active — galaxies: Seyfert — X-rays: galaxies

## 1. Introduction

X-ray observations can provide constraints on physical conditions in the innermost regions of Active Galactic Nuclei (AGN), as the X-rays are generally thought to originate very close to the central engines. On the basis of spectroscopic observations, the leading models of the X-ray continuum production are generally based on a hot, Comptonizing electron or electron-positron pair corona above the accretion disk which multiply-upscatters thermal soft photons from the disk to produce an X-ray power-law in the energy range 1-100 keV (e.g., Haardt, Maraschi & Ghisellini 1994). Furthermore, the disk, or some other cold, optically thick material, reprocesses the hard X-rays, as evidenced by the so-called 'Compton reflection humps' above  $\sim 10$  keV in Seyfert 1

spectra, as well as strong iron fluorescent lines at  $\sim 6.4$  keV (Lightman & White 1988, Guilbert & Rees 1988, Pounds et al. 1990). AGN also exhibit rapid, aperiodic variability, for which no fully satisfying explanation has been advanced. However, at least on short time scales, the variability amplitude has long been known to correlate inversely with the source luminosity for normal Seyfert 1s (e.g., Barr & Mushotzky 1986, Lawrence & Papadakis 1993, Nandra et al. 1997).

Probably the best way to characterize AGN variability, if adequate data exist, is to measure the fluctuation power density spectra (PDS). On short time scales ( $\lesssim 1$  d), *EXOSAT* showed that AGN PDS are well-described as power-laws ( $P \propto f^s$ , where  $P$  is the power at temporal frequency  $f$ ), with index  $s = -1$  to  $-2$  (e.g., Green, McHardy & Letho 1993, Lawrence & Papadakis 1993). However, only the *Rossi X-ray Timing Explorer (RXTE)*, with its combination of flexible scheduling, relaxed pointing constraints, high throughput and rapid slew speed, has been able to monitor AGN variations over long time scales. Only one Seyfert 1 galaxy, NGC 3516, has been subjected to a combination of even sampling on long, medium and short time scales needed to produce the first AGN PDS to span time scales of minutes to months. This PDS showed a flattening on a time scale of  $\sim 1$  month (Edelson & Nandra 1999). Unfortunately, the *RXTE* archives do not currently contain adequate data to measure such detailed PDS for other AGN, although it is expected that the current round of observations will make this feat possible within a few years.

However, the archived data can be used for a less detailed study of the long-term continuum variability properties of Seyfert 1s. This paper presents the first such study, a survey of homogeneously-sampled,  $\sim 300$  day light curves of nine Seyfert 1s observed by *RXTE*. The data reduction and sampling are described in § 2 and the analysis is described in § 3. As discussed in § 4, this has allowed significant insight into AGN variability, such as quantifying the relation between source luminosity and PDS cutoff frequency. Furthermore, the long-term spectral variability properties can be used to test spectral formation models. A short summary is given in § 5.

## 2. Data Collection and Reduction

*RXTE* observed  $\sim 105$  AGN for a total of  $\sim 13$  Msec during the first 3 years of its mission (calibration phase and Cycles 1-3). Almost all of these data had become public by the time that these analyses were performed (February 2000). This paper utilized these data as well as the authors' proprietary observations of five Seyfert 1s observed during Cycle 4. Section 2.1 describes the reduction of the *RXTE* data set used in this paper.

The goal of this project was to obtain long time scale monitoring sampled as uniformly as possible for as large a number of objects as possible. Optimizing this tradeoff for the currently available archive yielded a sample of nine Seyfert 1s that were sampled an average of once every 5–13 days for a total period of 300 days, along with adequate short time scale *ASCA* data. The construction of this sample is described in §2.2. The *ASCA* data and analysis are discussed in §2.3.

## 2.1. *RXTE* Data

The *RXTE*'s Proportional Counter Array (PCA) consists of five identical proportional counter units (PCUs; see Swank 1998). For simplicity and uniformity, data were collected only from those PCUs that did not suffer from repeated breakdown during on-source time (PCUs 0 and 2 for the entire data set, plus PCU 1 for observations prior to 1998 December). All quoted count rates for this paper are normalized to 1 PCU. The data were reduced using standard extraction methods and FTOOLS v4.2 software. Data were rejected if they were gathered less than  $10^\circ$  from the Earth's limb, if they were obtained within 30 min after the satellite's passage through the South Atlantic Anomaly (SAA), if `ELECTRON0`  $> 0.1$ , or if the satellite's pointing offset was greater than  $0.02^\circ$ .

As the PCA has no simultaneous background monitoring capability, background data were estimated by using `PCABACKEST v2.1B` to generate model files based on the particle-induced background, SAA activity, and the diffuse X-ray background. This background subtraction is the dominant source of systematic error in *RXTE* AGN monitoring data. The background models are best calibrated for the topmost PCU layer, so only counts extracted from this layer were used; restricting to the topmost layer also maximized the signal-to-noise ratio. All of the targets were faint ( $< 40 \text{ ct s}^{-1} \text{ PCU}^{-1}$ ), so the applicable 'L7-240' background models were used. Because the PCU gain settings changed three times since launch, the count rates were rescaled to a common gain epoch. Light curves binned to 16 s were generated for all targets over the 2-10 keV bandpass, where the PCA is most sensitive and the systematic errors and background are best quantified. Light curves were also generated for the 2-4 keV and 7-10 keV bands. The data were then binned on orbital time scales; orbits with less than 10 points were rejected. Errors on each point were obtained from the standard deviations of the data in each orbital bin. Further details of *RXTE* data reduction can be found in, e.g., Edelson & Nandra (1999).

## 2.2. Optimized Sampling and Source Selection

The main goal of this project was to understand the long-term X-ray variability properties of Seyfert 1s. This required producing a substantial sample of objects that were (to the greatest degree possible) uniformly monitored on long time scales for good comparison between sources. Furthermore, there was required to exist adequate short-term data for comparison of the two time scales. Objects were also required to contain at least 20 points in the final light curve. Sources with a weighted mean count rate significantly below  $1 \text{ ct s}^{-1} \text{ PCU}^{-1}$  over the full 2-10 keV bandpass were rejected to minimize the risk of contamination from faint sources in the field-of-view and to ensure adequate signal-to-noise.

The sampling of the publically available Cycle 1-3 data was highly uneven in general, as observations were made with a wide variety of science goals. The resulting light curves featured a wide range of sampling patterns and durations. Targets with observations that spanned less than

the optimum window of  $\sim 300$  d were rejected. Choosing a longer window would have resulted in too few sources in the final survey, and a shorter window would have been less appropriate for long-term variability analysis, as many sources had  $\sim 2$  month gaps of 1-year time scales due to satellite  $\beta$ -angle viewing constraints. Targets with gaps greater than 33% of the total duration were also rejected, as gaps reduce the statistical significance of parameters derived over the full duration. For each target, the most densely sampled 300 d that did not include significant gaps was selected for analysis.

To extract a data set that was as uniformly sampled as possible, it was necessary to resample at a common, optimized sampling rate. This was done with an algorithm that kept spaces between adjacent accepted points as close to 5 d as the original sampling pattern allowed. Resampling at a rate longer than 5 d would have resulted in too few points in the final light curves, while resampling significantly more frequently would have yielded light curves that were not sufficiently uniformly sampled a data set given the original range of sampling patterns.

This reduction yielded a sample of fifteen AGN, including two Seyfert 2s (NGC 4258 and NGC 5506) and four blazars (3C 273, 3C 279, 3C 454.3 and PKS 1510-089) that will not be considered further in this paper. Excluding those objects yielded a sample of nine Seyfert 1s (3C 120, Ark 120, Fairall 9, MCG-6-30-15, NGC 3516, NGC 3783, NGC 4051, NGC 4151, and NGC 5548). Figure 1 shows the full 2-10 keV light curves for these Seyfert 1s, ranked by source luminosity. Figure 2 shows the light curves after applying the  $\sim 300$  d window and resampling. Table 1 summarizes the source observation and sampling parameters for the survey targets over the 2-10 keV bandpass. All source fluxes were calculated using HEASARC’s online W3PIMMS v3.0 Flux Converter assuming an intrinsic power-law with a photon index obtained from the online Tartarus archive of *ASCA* AGN observations (<http://tartarus.gsfc.nasa.gov>; e.g. Nandra et al. 1997, Turner et al. 1999). Luminosities were calculated assuming  $H_o = 75 \text{ km s}^{-1} \text{ Mpc}^{-1}$  and  $q_o = 0.5$ .

### 2.3. *ASCA* Data

Short-term 2-10 keV light curves were also obtained from the Tartarus database. The count rates in the light curves provided had been combined and averaged between *ASCA*’s two Solid-state Imaging Spectrometers (SIS; Burke et al. 1994, Gendreau 1995) and binned to 16 s. For each target, the observation with the longest duration available in the archive was selected, and only the first 1 day (maximum duration of 86.4 ks) was used for these analyses. The light curves were rebinned on orbital time scales with the same algorithm used for the *RXTE* data to yield light curves that were generally 10-15 consecutive orbital bins. Background light curves were similarly binned and subtracted to produce net count rate light curves. Table 2 lists the source observation and sampling parameters for the *ASCA* data.

### 3. Analysis

#### 3.1. Excess Variance

The normalized excess variance,  $\sigma_{RMS}^2$ , was utilized to quantify the amplitude of variability in each light curve (e.g., Nandra et al. 1997):

$$\sigma_{RMS}^2 = \frac{1}{N\mu^2} \sum_{i=1}^N [(X_i - \mu)^2 - \sigma_i^2]$$

where the count rates for the  $N$  points in each light curve are  $X_i$ , with errors  $\sigma_i$ , and  $\mu$  is the unweighted arithmetic mean. Table 3 lists the excess variances for each target over the 2-4 keV band, 7-10 keV band, and full 2-10 keV bandpass for the *RXTE* data, the ratio of the 300 d 2-4 keV to 7-10 keV variances, and excess variances over the full 2-10 keV bandpass for the *ASCA* data, ( $\sigma_{300d,soft}^2$ ,  $\sigma_{300d,hard}^2$ ,  $\sigma_{300d}^2$ ,  $\sigma_{soft}^2/\sigma_{hard}^2$ , and  $\sigma_{1d}^2$ , respectively).

#### 3.2. Construction of Correlation Diagrams

Figure 3 displays the excess variance for both the long (300 day) and short (1 day) time scale data plotted against source luminosity over the 2-10 keV bandpass. For all sources, the long-term excess variances are greater than the short-term excess variances. Both data sets conform well to a power-law of the form  $\sigma_{RMS}^2 \propto L_x^{-a}$ , an anticorrelation observed before in AGN (e.g. Green, McHardy, & Lehto 1993, Nandra et al. 1997, Turner et al. 1999). The nine short-term data points were fitted by a logarithmic slope  $a = 0.861 \pm 0.070$ . The long-term data are described by a power-law with a much shallower slope,  $a = 0.277 \pm 0.009$ . The correlation is much stronger for the long-term data (with a correlation coefficient of  $r = -0.972$ ) than for the short-term data (where  $r = -0.839$ ).

The zero-lag correlation between  $\sigma_{300d,soft}^2$  and  $\sigma_{300d,hard}^2$  is shown in Figure 4. All of the sources exhibit stronger variability in the relatively softer X-rays than in the harder X-rays, as the slope of the best-fit line is  $0.724 \pm 0.041$ , indicating that the soft X-rays make an increasingly dominant contribution to the overall variability for the more variable sources.

Another test of spectral variability is to plot the 7-10 keV count rates against the 2-4 keV count rates for individual sources (see Figure 5). The resulting spectral variability slopes, listed in Table 3, range from 1.14 to 1.81, again indicating that the relatively soft band is more strongly variable.

Figure 6 plots this spectral variability slope against source luminosity and  $\sigma_{300d}^2$ . There is weak evidence for an anticorrelation between the spectral variability slope and source luminosity in the sense that less luminous sources exhibit more variability in the soft band. There is weak evidence for a positive correlation between the spectral variability slope and 2-10 keV  $\sigma_{300d}^2$ .

Table 4 summarizes the correlations discussed in this section.

## 4. Discussion

On long time scales, the anticorrelation between source luminosity and variability is stronger (higher correlation coefficient), yet shallower in power-law slope, compared to short time scales. The shallower slope on long time scales can be viewed as the highest luminosity sources showing the greatest increase in long-term variability amplitude. As discussed below, this trend can be explained by a simple scaling of PDS turnover frequency with luminosity. Furthermore, all of the targets exhibit stronger variability at relatively softer X-ray energies (2–4 keV) than at harder X-ray energies (7–10 keV), which allows tests of simple X-ray reprocessing models.

### 4.1. Variability-Luminosity Relationship and PDS Movement

As mentioned in the introduction, only one AGN (NGC 3516) currently has adequate data to clearly measure a cutoff in the PDS (at a time scale of  $\sim 1$  month; Edelson & Nandra 1999). A toy model can be constrained assuming that all AGN PDS have a universal shape, with the location of the break (in both amplitude and time scale) changing with luminosity. The observed anticorrelation between source luminosity and variability amplitude observed on short time scales (e.g., Lawrence & Papadakis 1993; Nandra et al. 1997) could then be due either to a positive correlation between luminosity and cutoff time scale or to an inverse correlation between luminosity and the overall variability amplitude. This is illustrated in Figure 7, with the first case of changing time scale shown on the left (e.g., less luminous sources vary more rapidly) and the second case of changing amplitude on the right (e.g., less luminous sources vary more strongly). It is also illustrated in Figure 8, except in  $f * P_f - f$  space instead of  $P_f - f$  space.

Within this model, it is possible to use the current data to discriminate between these two pictures. If the amplitude scales with luminosity but is independent of time scale, then the ratio of short- to long-term variances,  $\sigma_{1d}^2/\sigma_{300d}^2$ , will remain independent of luminosity. However, if the time scale changes with luminosity, then  $\sigma_{1d}^2/\sigma_{300d}^2$  will be larger for more luminous sources. Figure 9 is such a plot of  $\sigma_{1d}^2/\sigma_{300d}^2$  as a function of luminosity, with the solid line derived by scaling the measured PDS of NGC 3516 (with a high-frequency slope of  $-1.76$  and turnover frequency of  $4 \times 10^{-7}$  Hz) linearly with luminosity in  $P_f - f$  space. The short-term variances were obtained by integrating between temporal frequencies of  $1 \text{ d}^{-1}$  and  $15 \text{ d}^{-1}$  (one satellite orbit). The long-term variances were calculated using the frequency range  $0.003 \text{ d}^{-1}$  to  $15 \text{ d}^{-1}$ . No arbitrary scaling was done. This result is roughly consistent with the idea that the variability time scale (the duration required for the source to achieve a given level of r.m.s. variability) is in proportion to the size of the emitting region in AGN and hence black hole mass, which in turn determines luminosity.

Finally, Figure 3 also shows that the long-term correlation is much stronger (more highly correlated) than the short-term correlation. This could be due to the a simple data effect: the long-term variability is stronger the short-term, and *RXTE* gets higher signal-to-noise ratios than *ASCA*. This would result in a higher variability-to-noise ratio for the long-term data, and therefore a stronger correlation.

#### 4.2. Spectral Variability results

Figures 4 and 5 demonstrate that all sources in the sample show stronger variability in the 2-4 keV band compared to the 7-10 keV band. This trend has been observed previously in Seyfert 1s, e.g., by Turner, George, & Nandra (1998). Green, McHardy, & Lehto (1993) model such spectral softening as the result of a constant reflection component superimposed on a variable soft component. However, this model is not consistent with the data reported in this paper. For the spectral model PEXRAV in XSPEC v11.00, consisting of an absorbed power-law plus Compton reflection component (Magdziarz & Zdziarski, 1995), the reflected component accounts for at most  $\sim 8\%$  of the total 7-10 keV flux. Assuming this maximum effect, a constant reflection component can reduce  $\sigma_{300\text{d,hard}}^2$  by as much as  $\sim 18\%$ . However, for all objects in the present sample,  $\sigma_{\text{soft}}^2/\sigma_{\text{hard}}^2$  is still larger than 1.18; as seen in Table 3, these values range from 1.30 to 3.85. This result suggests that the observed spectral variability may instead be due to changes in the intrinsic spectral slope  $\Gamma$ .

Haardt, Maraschi, & Ghisellini (1997) discuss a model for Comptonizing coronae in which optical depth variations in a fixed-geometry, plane-parallel, pair-dominated, optically thin ( $0.1 \leq \tau \leq 1.0$ ) corona drive spectral changes in the Comptonized emission in that spectral steepening and a decrease in corona temperature accompany increases in optical depth. The model predicts that a steepening of  $\Gamma$  by 0.2 over the 2-10 keV bandpass corresponds to an increase in 2-10 keV flux by a factor of 10 (valid for  $\Gamma \lesssim 2.0$ ). Assuming that the Comptonized power-law pivots at an energy of 10 keV, the 2-4 keV flux is therefore expected to increase by 25% more than the 7-10 keV flux increases. However, this model also is inconsistent with the data. The average increase of 2-10 keV flux for all targets in the present sample from the lowest to highest flux states is a factor of  $\sim 4$ ; scaling the model's prediction accordingly implies  $\Delta\Gamma = +0.12$ , and hence the 2-4 keV flux should increase by 14% relative to the 7-10 keV flux. For the present sample, however, the average increase is 53% (see Figure 5). There is more spectral variability and less total (2-10 keV) flux variability than the model predicts. Reasons for this discrepancy include the possibility that pairs may not dominate in coronae. However, Haardt, Maraschi, & Ghisellini (1997) also find that for a pair-dominated corona in which variations of the scale size of the corona are important and intrinsic flux variations are negligible, significant spectral variations could be expected without large variations in the 2-10 keV flux. This situation, which could arise from a corona composed of many active regions instead of a single homogeneous region, is more consistent with the present observations.

## 5. Conclusions

This paper reports the first X-ray variability survey with highly uniform and consistent sampling to probe long time scales ( $\sim 300$  d) in a reasonably large sample of Seyfert 1 galaxies. The variability amplitudes were found to be greater on long time scales than on short time scales, with the largest increases seen in the most luminous sources. This resulted in the slope of the anticorrelation between excess variance and luminosity being shallower on long time scales. This trend can be explained if the time scale for a variability mechanism increases for more luminous sources, as would be the case if all Seyfert 1s radiate at approximately the same ratio of  $L/L_{\text{Edd}}$ . Consequently, a PDS corresponding to a higher luminosity object will be displaced towards lower temporal frequencies relative to that of a lower luminosity object.

All of the Seyfert 1s exhibited stronger variability in the relatively soft 2-4 keV band than in the harder 7-10 keV band, too strong to be explained by a simple model based on the dilution of the power-law continuum in the 7-10 keV band by a constant Compton reflection component. The data are also inconsistent with a simple model of a static, pair-dominated, plane-parallel Comptonizing corona.

Recently, systematic monitoring with *RXTE* has been started for several Seyfert 1s, with even sampling over a wide range of time scales in the same pattern as the NGC 3516 campaign. When these campaigns are completed in 2002, it should be possible to measure the PDS over four decades of temporal frequency, hopefully allowing direct measurement of the turnover and determination of how PDS shape evolves with luminosity, as predicted in this paper.

The authors would like to thank Tess Jaffe and Simon Vaughan for help with data analysis. This work has made use of data obtained through the High Energy Astrophysics Science Archive Research Center Online Service, provided by the NASA Goddard Space Flight Center, the TARTARUS database, which is supported by Jane Turner and Kirpal Nandra under NASA grants NAG 5-7385 and NAG 5-7067, and the NASA/IPAC Extragalactic Database which is operated by the Jet Propulsion Laboratory, California Institute of Technology, under contract with the National Aeronautics and Space Administration. The authors acknowledge financial support from NASA grants NAG 5-7315 and NAG 5-9023.

## REFERENCES

- Barr, P., & Mushotzky, R., 1986, *Nature*, 320, 421
- Burke, B. E., Mountain, R. W., Daniels, P. J., & Dolat, V. S., 1994, *IEEE Trans. Nuc. SCI.* 41, p. 375
- Edelson, R. & Nandra, K. 1999. *ApJ*, 514, 682
- Gendreau, K. 1995. Ph.D. thesis, Massachusetts Institute of Technology



- Green, A., McHardy, I., & Lehto, H., 1993, MNRAS, 265, 664
- Guilbert, P., & Rees, M., 1988, MNRAS, 233, 475
- Haardt, F., Maraschi, L., & Ghisellini, G., 1994, ApJ, 432, L95
- Haardt, F., Maraschi, L., & Ghisellini, G., 1997, ApJ, 476, 20
- Lawrence, A., & Papadakis, I., 1993, ApJ, 414, L85
- Lightman, A., & White, T., 1988, ApJ, 335, 57
- Magdziarz, P., & Zdziarski, A., 1995, MNRAS, 273, 837
- Nandra, K., George, I., Mushotzky, R.F., Turner, T.J., & Yaqoob, T., 1997, ApJ, 476, 70
- Pounds, K., Nandra, K., Stewart, G., George, I., & Fabian, A., 1990, Nature, 344, 132 & Begelman, M., 1995, ApJ, 449, L13
- Swank, J., 1998, in Nuclear Phys. B (Proc. Suppl.): The Active X-ray Sky: Results From BeppoSAX and Rossi-XTE, Rome, Italy, 1997 October 21-24, eds. L. Scarsi, H. Bradt, P. Giommi, & F. Fiore (The Netherlands: Elsevier Science B.V.)
- Turner, T. J., George, I. M., & Nandra, K., 1998, ApJ, 508, 648
- Turner, T. J., George, I. M., Nandra, K., & Turcan, D., 1999, ApJ, 524, 667

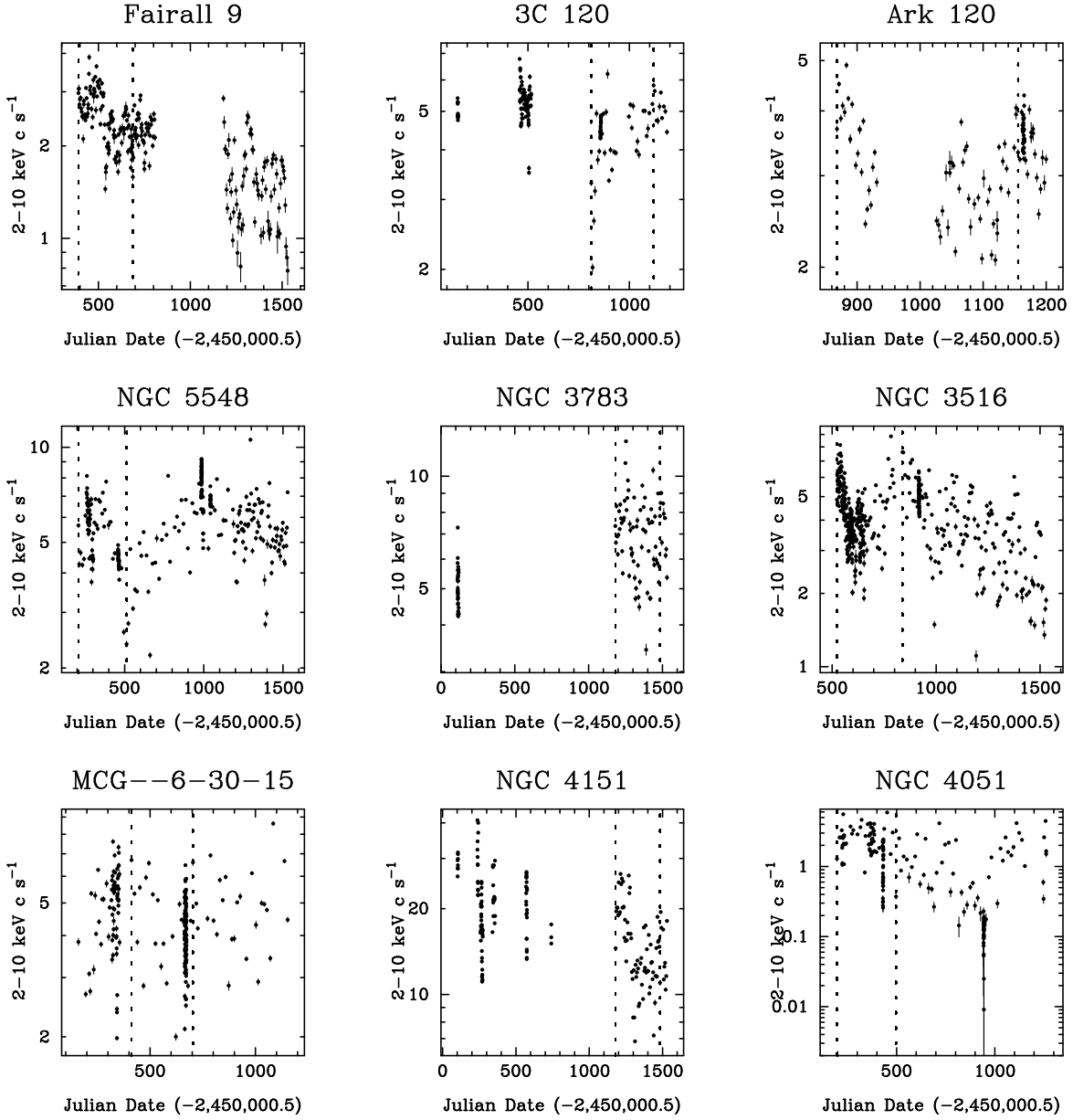


Fig. 1.— *RXTE* 2-10 keV light curves, ranked by luminosity, before applying the  $\sim 300$  d window and subsampling. Error bars are  $1\sigma$ . The dashed vertical lines indicate the  $\sim 300$  d period used for analysis.

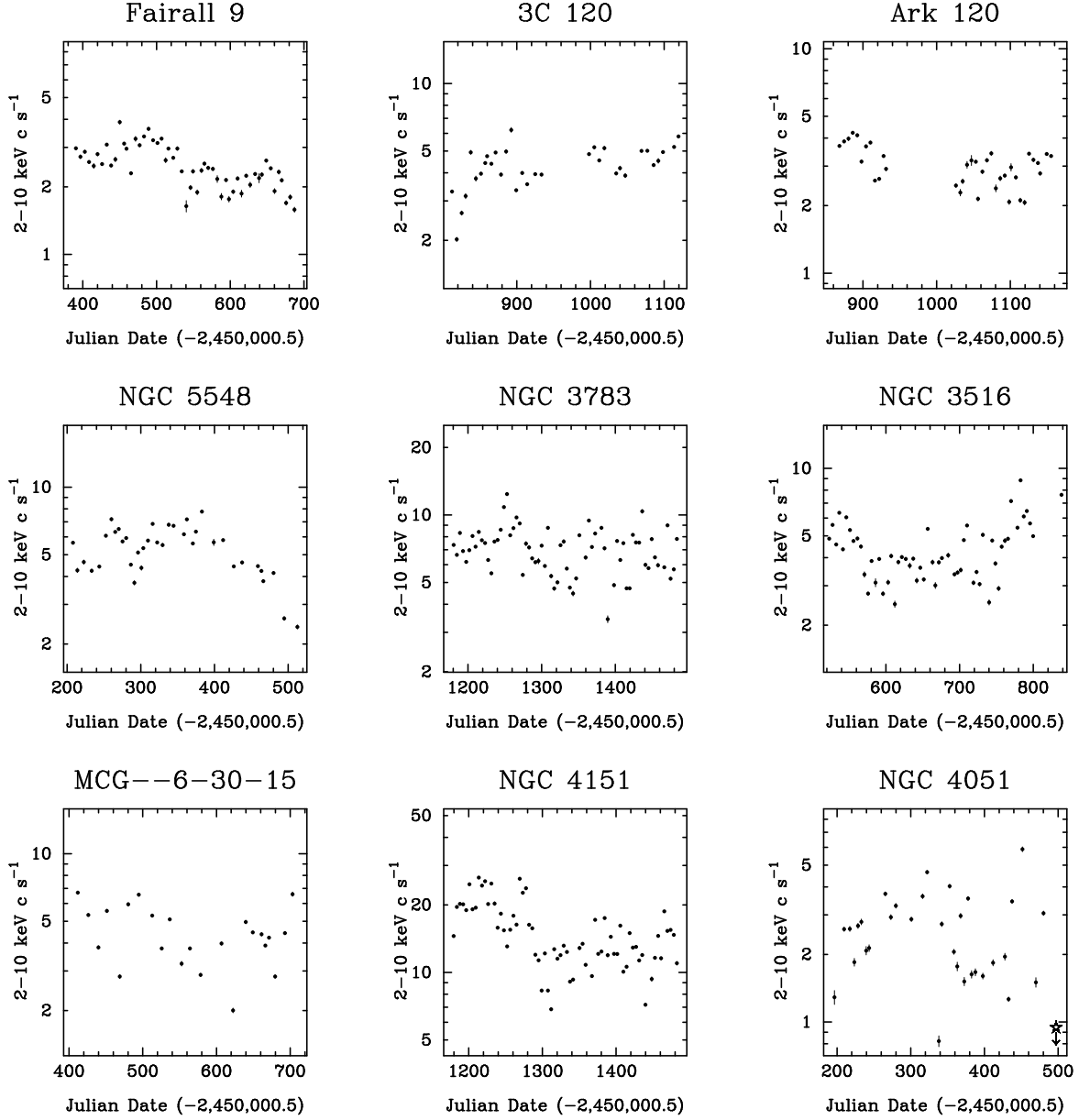


Fig. 2.— *RXTE* 2-10 keV light curves, ranked by luminosity, after applying the  $\sim 300$  d window and subsampling to 5 d. Error bars are  $1\sigma$ . The y-axis has been scaled such that the maximum and minimum values are, respectively, 3.5 and  $(3.5)^{-1} \times$  the mean count rate. A data point in NGC 4051 corresponding to  $\text{JD} - 2,450,000.5 = 497.30$ , rate =  $0.37 \pm 0.03$  has been omitted.

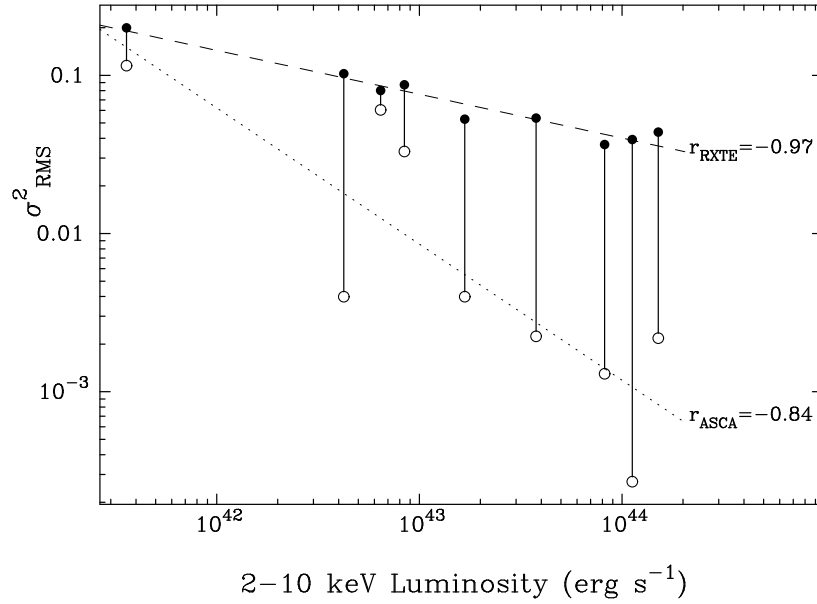


Fig. 3.— *RXTE* long-term excess variance and *ASCA* short-term excess variance plotted against source luminosity over the 2-10 keV bandpass. Filled circles, best-fit by the dashed line, are *RXTE* data; open circles, best-fit by the dotted line, are *ASCA* data. Note the tighter correlation in the *RXTE* data points.

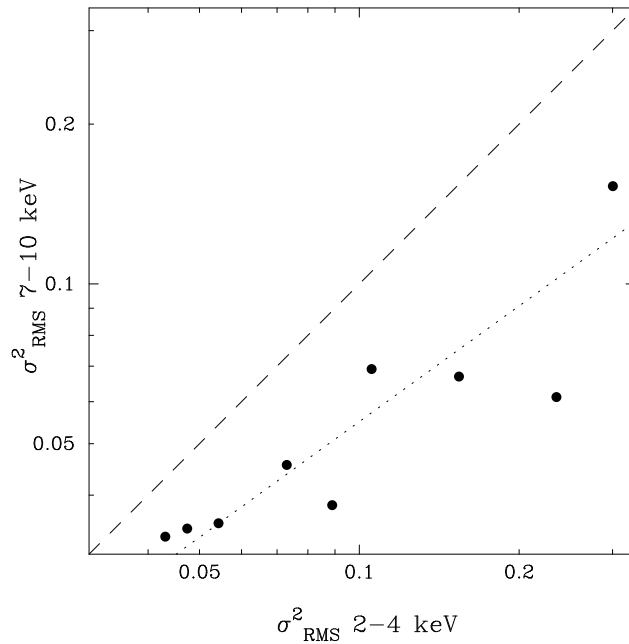


Fig. 4.— *RXTE* hard X-ray excess variance plotted against soft X-ray excess variance. A source with equally strong variability in the hard and soft bands would lie on the dotted line. All of the sources exhibit stronger variability in softer X-rays than in hard X-rays.

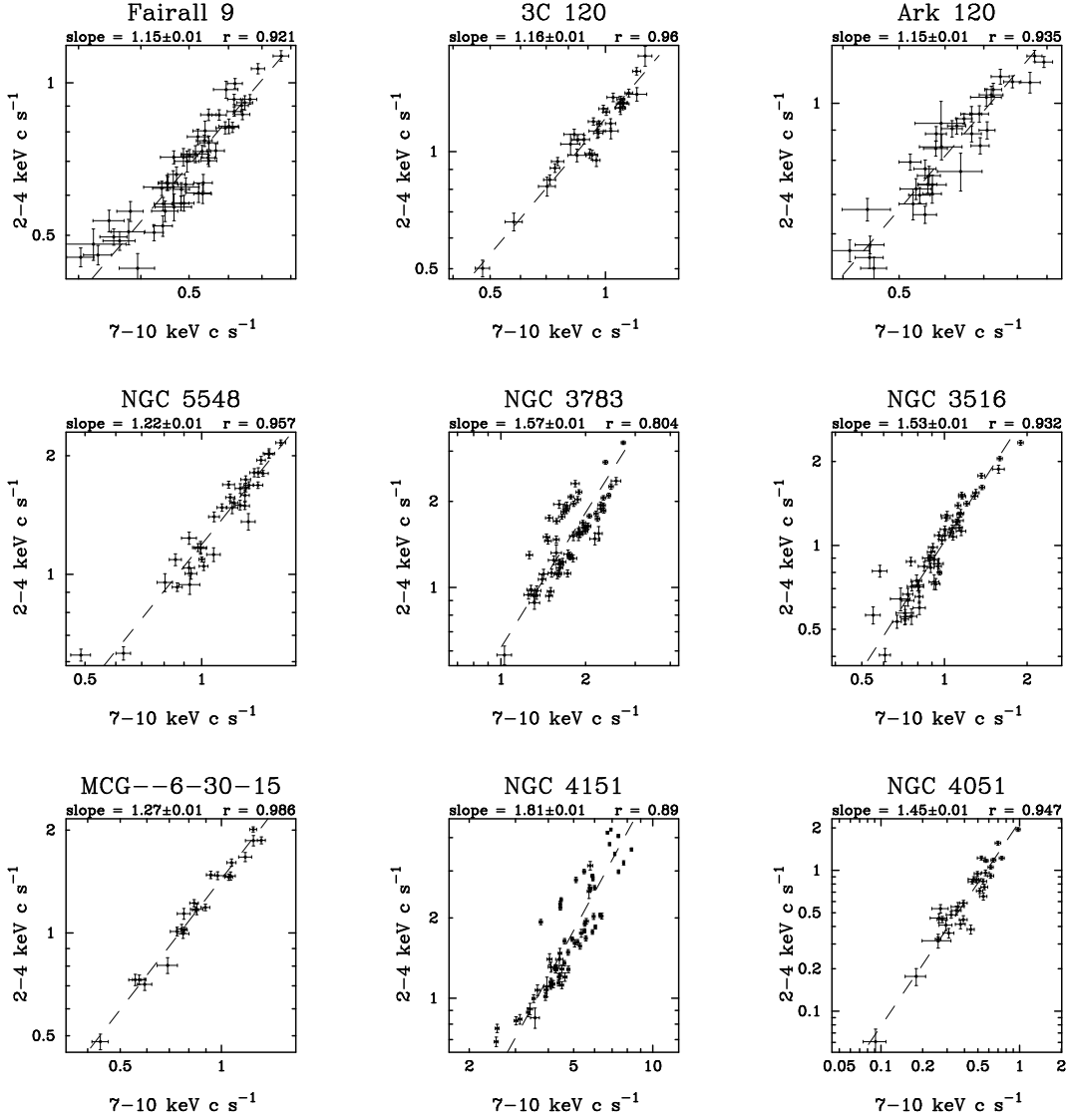


Fig. 5.— *RXTE* 2-4 keV count rates plotted against 7-10 keV count rates for the clipped and subsampled light curves, in order of descending 2-10 keV source luminosity. The resulting slope, described by the best-fit dashed lines, is the spectral variability slope.  $r$  is the correlation coefficient for each plot.

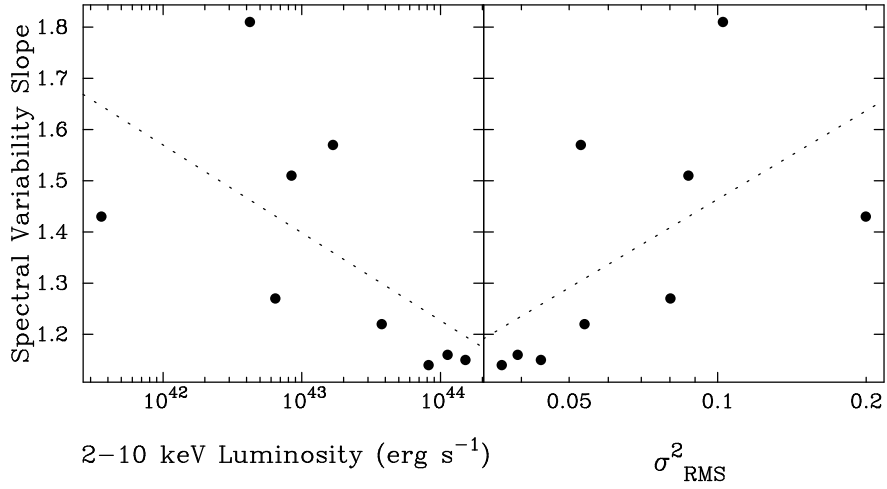


Fig. 6.— Spectral variability slope plotted against 2-10 keV source luminosity (left) and *RXTE* 2-10 keV long-term excess variance (right). In each plot, the dotted line indicates the best-fit line.

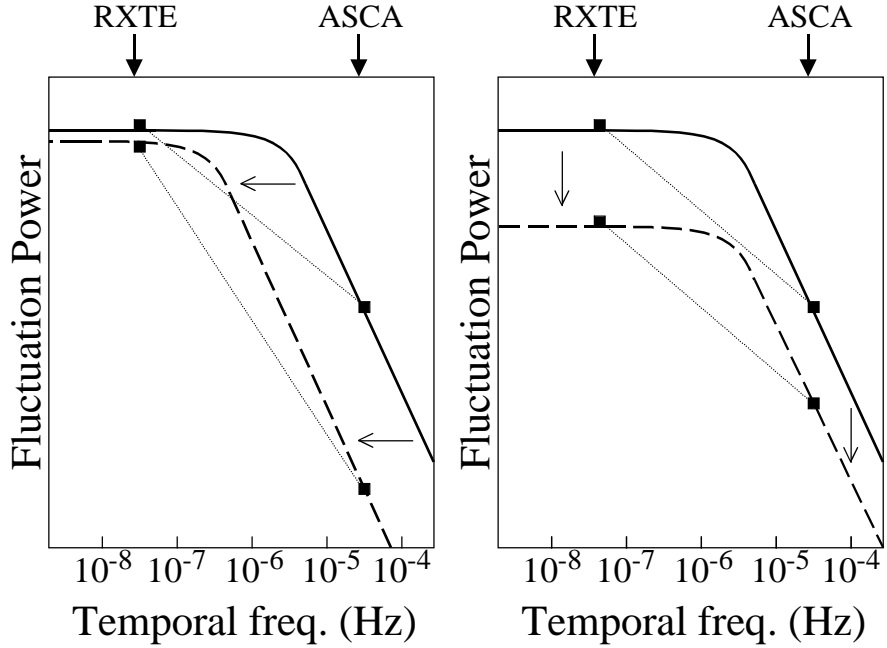


Fig. 7.— Model of a characteristic PDS change with increasing source luminosity, plotted in  $P_f - f$  space; the dashed-line PDS corresponds to a source with higher luminosity than the source corresponding to the solid-line PDS. If the PDS moves to the left in temporal frequency (left), then the ratio of low-frequency variability to high-frequency variability will be greater than in lower luminosity sources. If the PDS moves downward in fluctuation power (right), then the ratios of low- to high-frequency variability should be equal and independent of luminosity.

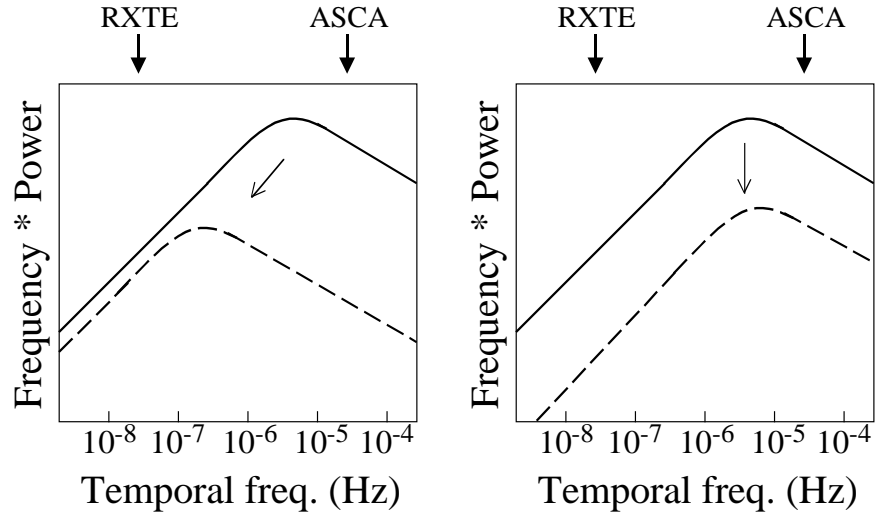


Fig. 8.— Model of a characteristic PDS change with increasing source luminosity, plotted in  $f * P_f - f$  space. The dashed-line PDS corresponds to a source with higher luminosity than the source corresponding to the solid-line PDS.

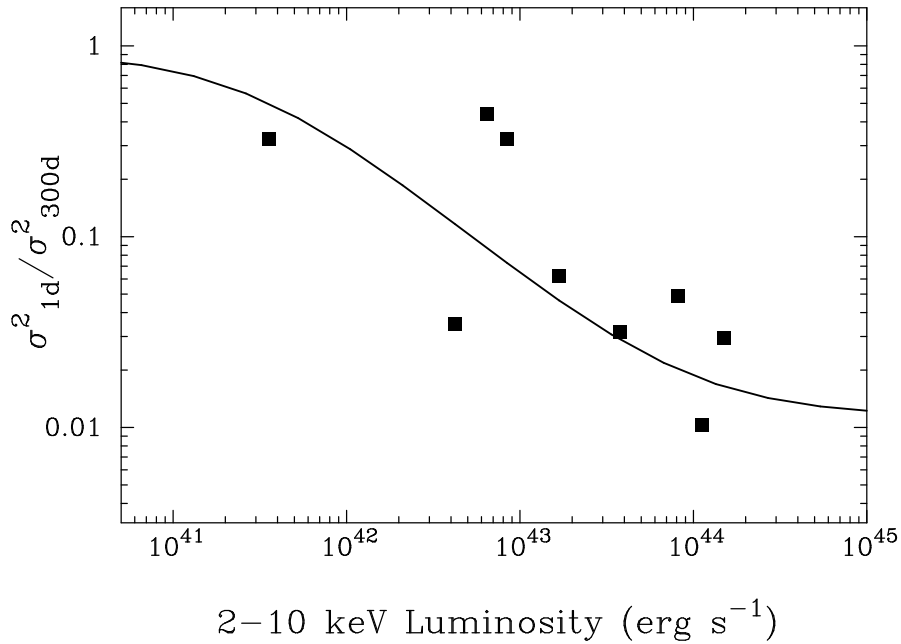


Fig. 9.— Predicted and measured values of  $\sigma_{1d}^2 / \sigma_{300d}^2$  (solid line and squares, respectively) plotted against luminosity. No arbitrary scaling was done.

Table 1. Source and *RXTE* Sampling Parameters

Name	$z$	Num. Points	JD-2450000.5 Range	Mean Count Rate (ct s <sup>-1</sup> )	Mean S/N	Lumin. $\log(L_{2-10 \text{ keV}})$ (erg s <sup>-1</sup> )
Fairall 9	0.047	54	50390.6-50687.2	2.5	56	44.18
3C 120	0.033	33	50812.1-51119.4	4.3	73	44.05
Ark 120	0.032	36	50868.1-51155.3	3.0	56	43.91
NGC 5548	0.017	37	50208.1-50512.6	5.1	77	43.58
NGC 3783	0.010	68	51180.6-51483.6	7.1	84	43.22
NGC 3516	0.009	57	50523.0-50838.3	4.4	69	42.93
MCG-6-30-15	0.008	23	50411.9-50703.3	4.3	71	42.81
NGC 4151	0.003	69	51179.6-51482.5	15.2	135	42.63
NGC 4051	0.002	33	50196.5-50497.3	2.4	37	41.55

Note. — All quantities are for the 2-10 keV bandpass. The targets are ranked by 2-10 keV luminosity. Redshifts (Column 2) were obtained from the NED database. Column 4 is the number of points in the *RXTE* light curve after clipping to  $\sim 300$  d and subsampling to 5 d. Column 5 is the weighted mean *RXTE* count rate per PCU.



Table 2. *ASCA* Sampling Parameters

Name	Num. Points	JD-2450000.5 Range	Sequence ID No.	Count Rate (ct s <sup>-1</sup> )	Mean S/N	Γ
Fairall 9	11	49700.6-49701.3	73011000	0.47	19	2.18
3C 120	15	49400.6-49401.6	71014000	0.94	35	1.97
Ark 120	15	49624.8-49625.8	72000000	0.55	25	2.02
NGC 5548	15	49195.6-49196.6	70018000	0.89	26	1.79
NGC 3783	11	50278.2-50278.9	74054020	1.31	30	1.43
NGC 3516	13	49444.1-49445.0	71007000	1.49	42	1.60
MCG–6-30-15	15	49556.2-49557.2	72013000	0.80	26	1.80
NGC 4151	15	49847.1-49848.1	73019000	1.96	62	0.45
NGC 4051	15	49510.6-49511.6	72001000	0.44	20	2.07

Note. — Column 1 is the number of points in the *ASCA* light curve after orbitally binning. Column 4 is the weighted mean *ASCA* count rate averaged between both SIS instruments. The photon indices in column 7 were obtained from the Tartarus database.

Table 3. Derived Variability Parameters

Name	$\sigma_{300d,soft}^2$ <i>RXTE</i> 2-4 keV	$\sigma_{300d,hard}^2$ <i>RXTE</i> 7-10 keV	$\sigma_{300d}^2$ <i>RXTE</i> 2-10 keV	$\sigma_{soft}^2/\sigma_{hard}^2$ <i>RXTE</i>	$\sigma_{1d}^2$ <i>ASCA</i> 2-10 keV	Spectral Variability Slope
Fairall 9	0.054	0.035	0.044	1.54	0.0022	1.15
3C 120	0.047	0.035	0.039	1.34	0.0003	1.16
Ark 120	0.043	0.033	0.037	1.30	0.0013	1.14
NGC 5548	0.073	0.046	0.054	1.59	0.0022	1.22
NGC 3783	0.089	0.038	0.053	2.34	0.0040	1.57
NGC 3516	0.154	0.067	0.087	2.30	0.0330	1.51
MCG–6-30-15	0.106	0.069	0.080	1.54	0.0604	1.27
NGC 4151	0.235	0.061	0.103	3.85	0.0040	1.81
NGC 4051	0.301	0.153	0.200	1.97	0.1153	1.43

Table 4. Summary of Correlations

Figure No.	x-axis	y-axis	r	P(r)	Slope
3	$\sigma_{300d}^2$	Luminosity	-0.972	$1.18 \times 10^{-5}$	$-0.277 \pm 0.009$
3	$\sigma_{1d}^2$	Luminosity	-0.839	$4.69 \times 10^{-3}$	$-0.861 \pm 0.070$
4	$\sigma_{300d,hard}^2$	$\sigma_{300d,soft}^2$	+0.887	$1.43 \times 10^{-3}$	$+0.724 \pm 0.041$
6	Luminosity	Spect. Var. Slope	-0.616	$7.73 \times 10^{-2}$	$-0.17 \pm 0.03$
6	Long-term $\sigma_{300d}^2$	Spect. Var. Slope	+0.586	$9.73 \times 10^{-2}$	$+0.57 \pm 0.10$

Note. — Luminosity is over the 2-10 keV bandpass. Short-term data taken from *ASCA*; all others from *RXTE*. Column 4 is the correlation coefficient. P(r) in column 5 is the probability of obtaining that correlation coefficient by chance.